

## The role of particle associated microbes in remineralization of fecal pellets in the upper mesopelagic of the Scotia Sea, Antarctica

Anna Belcher,<sup>\*1,2</sup> Morten Iversen,<sup>3,4</sup> Clara Manno,<sup>5</sup> Stephanie A. Henson,<sup>1</sup>  
Geraint A. Tarling,<sup>5</sup> Richard Sanders<sup>1</sup>

<sup>1</sup>Ocean Biogeochemistry and Ecosystems, National Oceanography Centre, European Way, Southampton, UK

<sup>2</sup>University of Southampton, Southampton, UK

<sup>3</sup>Helmholtz Young Investigator Group SEAPUMP, Alfred Wegener Institute for Polar and Marine Research, Bremerhaven, Germany

<sup>4</sup>MARUM, University of Bremen, Bremen, Germany

<sup>5</sup>Ecosystems, British Antarctic Survey, Natural Environment Research Council, Cambridge, UK

### Abstract

Fecal pellets (FP) are a key component of the biological carbon pump, as they can, under some circumstances, efficiently transfer carbon to depth. Like other forms of particulate organic carbon (POC), they can be remineralized in the ocean interior (particularly in the upper 200 m), or alternatively they can be preserved in the sediments. The controls on the attenuation of FP flux with depth are not fully understood, in particular, the relative contributions of zooplankton fragmentation and microbial/zooplankton respiration to FP loss. Collection of sinking particles using Marine Snow Catchers at three ecologically contrasting sites in the Scotia Sea, Antarctica, revealed large differences in POC flux composition (5–96% FP) and flux attenuation despite similar temperatures. To determine the importance of microbial respiration on FP loss in the upper mesopelagic, we made the first ever measurements of small scale oxygen gradients through the boundary layer at the interface of krill FP collected from the Scotia Sea. Estimated carbon-specific respiration rates of microbes within FP ( $0.010\text{--}0.065\text{ d}^{-1}$ ) were too low to account for the observed large decreases in FP flux over the upper 200 m. Therefore, the observed rapid declines in downward FP flux in the upper mesopelagic are more likely to be caused by zooplankton, through coprophagy, coprorhexy, and coprochaly. Microbial respiration is likely to be more important in regions of higher temperatures, and at times of the year, or in depths of the ocean, where zooplankton abundances are low and therefore grazing and fragmentation processes are reduced.

The biological carbon pump drives the transfer of carbon from the atmosphere, through the ocean interior and ultimately to the deep ocean and sediments (Volk and Hoffert 1985), reducing levels of carbon dioxide ( $\text{CO}_2$ ) in the atmosphere. However, of the  $5\text{--}20\text{ GtC yr}^{-1}$  that is estimated to be exported out of the euphotic zone globally (Henson et al. 2011), only a minor fraction reaches the sea bed. The reduction in particulate organic carbon (POC) flux with depth (attenuation) is particularly rapid in the upper mesopelagic, driven by

microbial remineralization, zooplankton grazing and, coprophagy (ingestion of fecal pellets (FP)), coprorhexy (fragmentation of FP), coprochaly (removal of FP membrane), as well as physical aggregation and disaggregation (Lampitt et al. 1990; Poulsen and Iversen 2008; Wilson et al. 2008; Turner 2015). However, the practical difficulties of making measurements in this dynamic region of the ocean mean that, despite the importance of remineralization depth to atmospheric  $\text{CO}_2$  levels (Kwon et al. 2009), the balance of processes determining POC flux attenuation are poorly understood (Giering et al. 2014).

The repackaging of phytoplankton, and loosely packed slow sinking aggregates, into fast sinking FP by zooplankton may increase greatly transfer efficiencies through the mesopelagic. FP can be a substantial component of deep sea sediment trap fluxes, but this contribution is highly variable, both spatially and temporally (Wilson et al. 2013; Manno et al. 2015; Turner 2015). Zooplankton may attenuate the flux of POC producing smaller, slower sinking particles more

\*Correspondence: A.belcher@noc.soton.ac.uk

This article was published online 11 February 2016. A footnote stating that some late changes updated in Table 1 after the early view publication. This notice is included in the online and print versions to indicate that both have been corrected.

This is an open access article under the terms of the Creative Commons Attribution License, which permits use, distribution and reproduction in any medium, provided the original work is properly cited.

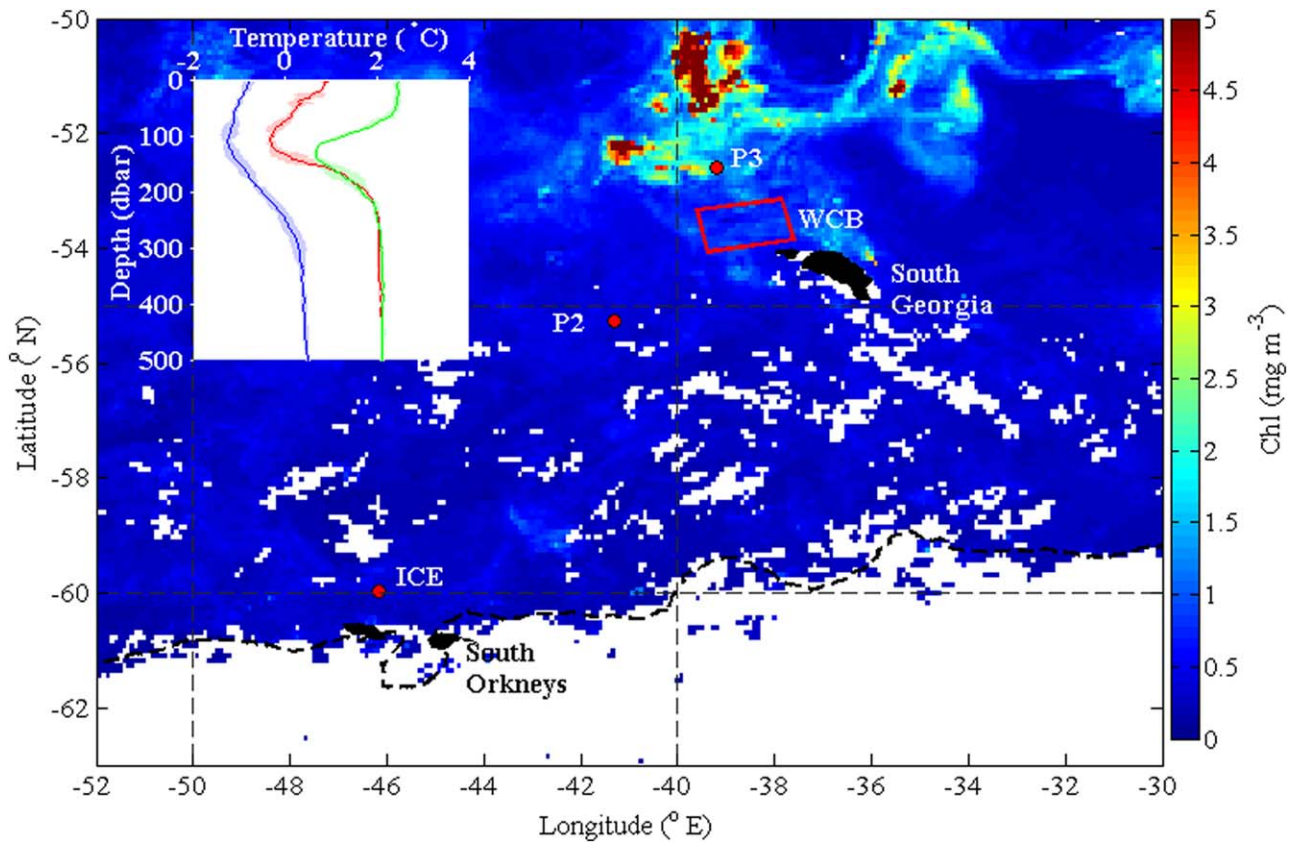


**Fig. 1.** Station locations (indicated by red circles and red square) overlain on MODIS Aqua satellite chlorophyll for December 2014. Position of ice edge on December 14<sup>th</sup> 2014 shown by black dotted line (OSTIA sea ice data). Inset displays vertical temperature profiles at ICE (blue), P2 (red) and P3 (green), lighter shades indicate standard deviations based on multiple deployments at each site.

readily accessible to marine microbes (Lampitt et al. 1990; Iversen and Poulsen 2007; Mayor et al. 2014). Temperature has also been identified as a main control on POC flux attenuation, with higher temperatures driving increased rates of heterotrophic respiration and high attenuation (Iversen and Ploug 2013; Marsay et al. 2015). However, it is not clear whether biological processes such as particle type and lability, and zooplankton fragmentation and grazing, therefore play a minimal role on flux attenuation, or whether temperature is acting as a proxy for these biological variations. To establish whether the temperature trend (Marsay et al. 2015) is applicable globally, these biological processes need to be investigated in regions where temperature is invariant.

Studies aiming to identify the main mechanisms controlling the retention of FP in the upper mesopelagic have drawn differing conclusions. Jing et al. (2012) found that FP are rapidly colonised by free living bacteria which may contribute significantly to their degradation, whereas Cnudde et al. (2013) suggest that degradation by bacteria packed inside the FP is equally important. Conversely, FP incubations performed by Poulsen and Iversen (2008) demonstrated that protozooplankton were the main driver of FP remineralization. More recently, it has been suggested that interactive

effects must be considered, with the mechanical break up of large FP by copepods supporting further degradation by dinoflagellates (Giering et al. 2014; Svensen et al. 2014).

Considering the important (and at times dominant) role that FP play in the transfer of carbon out of the upper ocean and to the deep sea, an improved understanding of the balance between zooplankton and microbial decomposition of FP within the mesopelagic is needed (Steinberg et al. 2008; Iversen et al. 2010; Giering et al. 2014). This requires not only knowledge of mesopelagic POC flux, but also the composition of sinking material, rates of microbial respiration on sinking particles, as well as concurrent information on ecosystem structure.

In this study, we measured particle flux and composition at a number of sites in the Scotia Sea, Antarctica. The Scotia Sea contains several diverse oceanographic regimes within a narrow range of temperatures, providing an ideal setting to assess the balance of microbial and zooplankton degradation processes without the added complication of temperature variability. We hypothesize that contrasting community structures will lead to differences in particle flux and flux attenuation, despite similar temperatures. We present the first direct measurements of microbial respiration rates of

*Euphausia superba* FP and use these rates to assess the balance between zooplankton and microbe driven flux attenuation processes in the upper mesopelagic.

### Materials and procedures

We measured total particle flux and oxygen concentration gradients of particles on *RRS James Clark Ross* cruise JR304 to the Scotia Sea, Antarctica in austral spring 2014 (Fig. 1). Samples were collected from three main sites, P2 and P3, upstream and downstream of South Georgia (at  $-55.248^{\circ}\text{N}$ ,  $-41.265^{\circ}\text{E}$  and  $-52.812^{\circ}\text{N}$ ,  $-39.972^{\circ}\text{E}$  respectively), and ICE ( $-59.962^{\circ}\text{N}$ ,  $-46.160^{\circ}\text{E}$ ). The ICE station was characteristic of the marginal ice zone with intermittent ice cover in the weeks prior to sampling. Additional FP were obtained from the Western Core Box site (Fig. 1). Vertical profiles of the water column at each site were made using a Conductivity-Temperature-Depth (CTD) unit (Seabird 9Plus with SBE32 carousel); these profiles were used to define the base of the mixed layer for further instrument deployments.

### Chlorophyll *a*

Water samples (300 mL) for Chl *a* were taken from the ship's uncontaminated underway supply (6 m) and the CTD rosette, filtered onto 0.8  $\mu\text{m}$  MPF300 glass fiber filters, and frozen at  $-20^{\circ}\text{C}$ . Samples were extracted in 90% acetone for 22–24 h at  $4^{\circ}\text{C}$  and fluorescence measured on a Trilogy Turner Designs 7200 lab fluorometer calibrated with a pure Chl *a* standard (Sigma, UK).

Aqua MODIS 9 km, eight day satellite Chl *a* data (downloaded from the NASA Ocean Biology website; <http://ocean-color.gsfc.nasa.gov/cms/>) were averaged over a 110 km  $\times$  110 km box ( $\sim 1^{\circ}$  latitude) centred on each station, to provide seasonal context and allow bloom timing to be inferred.

### Particle flux and composition

Sinking marine particles were collected using marine snow catchers (MSC), large (95 L) PVC closing water bottles designed to minimise turbulence (Riley et al. 2012). MSCs were deployed in rapid succession at 10 m and 110 m below the base of the mixed layer depth (MLD), identified from the most recent CTD profile, herein referred to as MLD+10 and MLD+110. This resulted in sampling between 39 m and 183 m. Our strategy of sampling at fixed depths relative to a variable MLD, rather than at absolute depths, allows comparison of export flux between sites (Buesseler and Boyd 2009). MSCs were deployed at 4–5 time points within a 36 h period at each station.

Following a two hour settling period (Riley et al. 2012), the particle collector tray (divided into four quadrants to allow sample splitting) was carefully removed from the base of the MSC and stored at  $4^{\circ}\text{C}$  for further analysis. The particles that sank fast enough to reach the particle collector tray in the 2 h settling period (here termed “fast sinking particles”), were picked from three quadrants using a wide-bore

pipette, filtered onto precombusted ( $450^{\circ}\text{C}$ , 24 h) glass fiber filters (25 mm diameter GF/F, Whatman), and oven dried at  $50^{\circ}\text{C}$  for replicate analysis of POC. Filters were subsequently fumed with 37% HCl in a vacuum desiccator for 24 h, and dried for 24 h at  $50^{\circ}\text{C}$ . Filters and filter blanks were placed in precombusted ( $450^{\circ}\text{C}$ , 24 h) tin capsules as in Hilton et al. (1986), and POC measured by a CE-440 Elemental analyser (Exeter Analytical.285 Inc).

Particles in the remaining quadrant were used to estimate sinking velocity and to make respiration rate measurements. POC fluxes ( $F$ ) were calculated as follows:

$$F \left( \text{mg m}^{-2} \text{ d}^{-1} \right) = \frac{\text{Mass}}{\text{Area}} \times \frac{w}{l} \quad (1)$$

where *mass* refers to the total mass (mg) of sinking POC collected from the MSC, *area* the area of the MSC opening based on inner MSC diameter, *w* the measured sinking velocity ( $\text{m d}^{-1}$ ), and *l* the length of the snow catcher (1.53 m). Particle sinking velocities of particles visible by eye (Equivalent Spherical Diameter (ESD)  $> 0.15$  mm) at each site were measured using a flow chamber (as for FP, see later section), and an average value for each site used for flux calculations. Flux attenuation was assessed via  $T_{100}$ , the ratio of POC flux at MLD+110 to the POC flux at MLD+10 (Buesseler and Boyd 2009). We have applied an exponential fit to our POC flux data and calculated the remineralization length scale ( $z^*$ ) (Boyd and Trull 2007):

$$F_z = F_0 \times \exp\left(\frac{z-z_0}{z^*}\right) \quad (2)$$

where  $z$  is the depth of the flux,  $F_0$  is flux at the reference depth (in this case MLD+10), and  $F_z$  the flux MLD+110. We also calculated attenuation coefficients ( $b$  values) following the commonly used method of Martin et al. (1987):

$$F_z = F_0 \times (z/z_0)^{-b} \quad (3)$$

High values of  $b$  are indicative of shallow remineralization and low values of deep remineralization. These methods of assessment of POC flux attenuation do not consider any in situ particle production between POC measurement depths and hence represent lower bound estimates of flux attenuation. In addition, they do not take into account addition or removal processes via lateral advection.

Additionally, at each site, particle composition was assessed through microscopic analysis of the collected sinking material. Particles were photographed using an Olympus SZX16 microscope with Canon EOS 60D camera and Olympus BX-SZX Micro Cam, and classified into: FP, fecal pellet fluff, phytodetrital aggregates, phytoplankton cells, zooplankton, lithogenic material, and unidentified phytodetritus. Phytodetrital aggregates were identified as aggregations  $> 0.1$  mm ESD containing phytoplankton cells and other

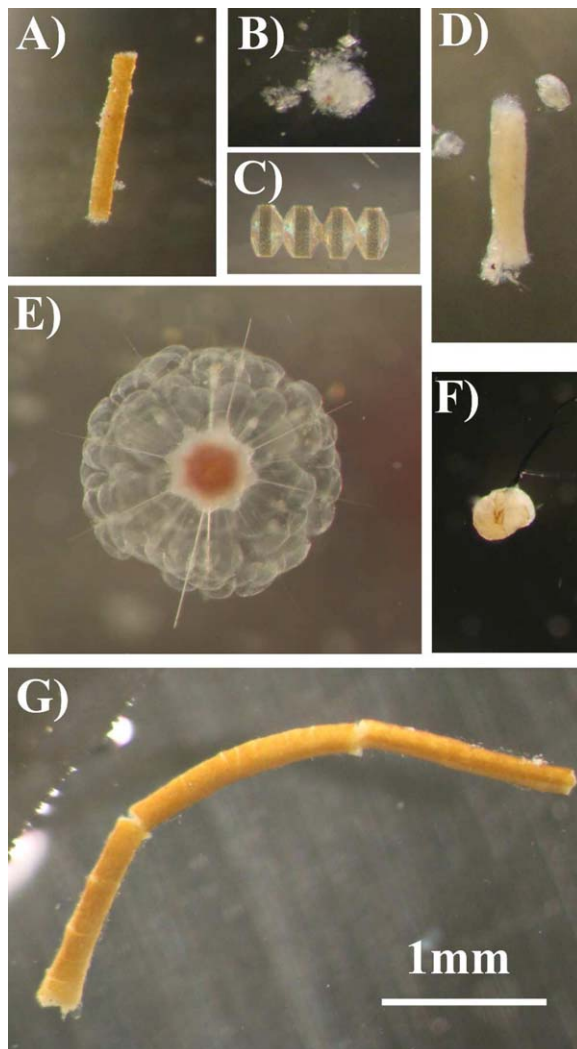


**Fig. 2.** Microscope photos of sinking material collected in marine snow catchers, (A) faecal pellet from ICE station, (B) marine snow aggregate from P2, (C) diatom chain from P2, (D) cylindrical faecal pellet from P2, (E) radiolarian from P2, (F) round faecal pellet from P2, (G) *E. superba* faecal pellet from Western Core Box Site. Scale bar refers to all photos.

phytodetrital material. Individual particle dimensions were measured using ImagePro and volumes calculated using formulae for a sphere, ellipsoid or cylinder depending on particle shape. Conversions from phytoplankton cell volume to carbon were based on the equation of Menden-Deuer and Lessard (2000) for diatoms  $>3000 \mu\text{m}^3$ :  $\log(\text{pgCcell}^{-1}) = -0.933 + 0.881 \cdot \log(\text{Volume} (\mu\text{m}^3))$ , and conversions from phytodetrital aggregate volume to carbon based on the equation of Alldredge (1998):  $\mu\text{C agg}^{-1} = 0.99 \cdot (\text{Volume} (\text{mm}^3))^{0.52}$ . The carbon content of FP was estimated based on POC to volume ratios calculated from FP collected during the research cruise (see following section). These size based estimates of POC content are associated with potentially large, but generally unquantifiable, uncertainties and

we suggest that carbon flux estimates are probably accurate to an order of magnitude. However, our usage of these parameterisations is consistent with previous studies (Alldredge 1998; Ebersbach et al. 2011; Laurenceau-Cornec et al. 2015) allowing comparisons to be made between sites.

#### Faecal pellet collection

Several methods were used to collect additional FP from the Scotia Sea for use in microbial respiration experiments. At the ICE station, paired motion-compensating Bongo nets (61 cm mouth diameter, 2.8 m long,  $100 \mu\text{m}$  and  $200 \mu\text{m}$  mesh) were deployed to 100–200 m and hauled vertically to the surface at about  $0.22 \text{ m s}^{-1}$ . This depth range encompasses the region where zooplankton populations are likely to be feeding and hence producing FP (Fielding et al. 2012; Ward et al. 2012a). FP believed to be from *E. superba* (Fig. 2G, assessed visually by a zooplankton taxonomist via comparison with FP from egestion experiments (see below)) were picked using a wide bore pipette, rinsed three times with filtered sea water and stored at  $4^\circ\text{C}$  until analysis (Fig. 2A). There is a chance that this rinsing may have removed some of the attached microbes from the particles which would result in an underestimation of respiration rates. Some FP were also collected using the MSC at P2 (e.g., Fig. 2D,F) at a depth of 45 m (just below the base of the mixed layer), where particle concentrations were expected to be higher (Prairie et al. 2013).

Additional FP for microbial respiration studies were obtained via targeted and nontargeted trawls for krill at the Western Core Box site (Fig. 1) using an RMT 8 (Rectangular Midwater Trawl, Roe and Shale 1979). This consists of two opening and closing nets (4 mm mesh) activated by a telemetering net monitor that provided real time information on water depth as well as environmental parameters such as temperature and salinity. Samples were obtained from two trawls performed in the upper 50 m of the water column, where krill populations are likely to reside at night (Fielding et al. 2012). Undamaged individuals of *E. superba* were carefully picked from the cod-ends and transferred into buckets containing surface seawater from the ship's underway system. The buckets were stored in a temperature controlled room ( $4^\circ\text{C}$ ) for 3–5 h to allow *E. superba* to egest their gut contents. FP were then carefully picked (Fig. 2G), rinsed three times with filtered sea water ( $0.22 \mu\text{m}$ ) and stored at  $4^\circ\text{C}$  until analysis. *E. superba* are a major component in the Scotia Sea ecosystem (Murphy et al. 2007), and the occurrence of large swarms (Fielding et al. 2012) have the potential to support POC transfer to the deep ocean through the production of large FP which can sink quickly through the mesopelagic (Atkinson et al. 2012; Manno et al. 2015).

#### Oxygen fluxes and respiration rates

Respiration rates of the microbial communities associated with FP (collected as described above) were calculated from direct measurements of oxygen gradients using microsensors and a temperature controlled flow chamber system (Ploug

and Jorgensen 1999). The flow chamber contained filtered sea water ( $0.22 \mu\text{m}$ ), taken from the MSC deployed at each site or the ship's underway system in the case of the Western Core Box. Within 24 h of collection, FP were placed carefully in the flow chamber, their  $x$ ,  $y$ , and  $z$  dimensions measured using a horizontal dissection microscope with a calibrated ocular, and three measurements of the sinking velocity made for each FP (Ploug et al. 2010). ESD was calculated based on cylindrical or spherical volumes.

The oxygen gradients (in steps of  $10\text{--}50 \mu\text{m}$ ) were measured through the diffusive boundary layer (DBL) downstream of the FP, between the FP surface and surrounding water using a Clark-type oxygen microelectrode with a guard cathode (Revsbech 1989) mounted in a micromanipulator. Net oxygen fluxes of sinking aggregates measured on the upstream and downstream side were previously shown not to be significantly different (Ploug and Jorgensen 1999). The surface of the FP was penetrated with the microsensors but complete profiles through the centre of the FP were often not possible due to FP stickiness, and the potential to damage the microsensors and break the FP. Despite the relatively small size of FP, thin DBLs and the dynamic nature of shipboard laboratory work, a total of 22 FP were measured, and 2–3 replicate profiles were taken for each FP where possible. Oxygen fluxes were calculated using a diffusion-reaction model based on Fick's first law of diffusion, using temperature and salinity corrected oxygen diffusion coefficients of  $1.171\text{--}1.253 \times 10^{-5} \text{ cm}^2 \text{ s}^{-1}$  based on experimental temperatures of  $3\text{--}5^\circ\text{C}$  (Broecker and Peng 1974). An Excel solver routine was utilized to find the optimum solution minimizing the sum of the squares between measured and modeled oxygen concentrations (see Ploug et al. 1997). Oxygen consumption in the DBL is a measure of the respiration rate of the microbial community associated with the FP due to the net exchange of oxygen via molecular diffusion. Total oxygen consumption within the FP was determined using geometric equations for the surface area of a cylinder, sphere or ellipsoid and carbon respiration calculated assuming a respiratory quotient of 1 mol  $\text{O}_2$  to 1 mol  $\text{CO}_2$  (Ploug et al. 1997; Ploug and Grossart 2000), which sits conservatively in the range of literature values typically applied (0.7–1.2) for respiration of carbohydrates and lipids (Berggren et al. 2012). Without more detailed knowledge of the exact composition of FP, or of the exact form of carbon utilized for microbial respiration, we believe this represents the best available estimate.

#### Fecal pellet POC content

Where it was possible to collect large numbers of FP, CHN analysis of FP POC content was conducted. Carbon to volume ratios were calculated from FP egested from krill captured in RMT 8 nets at the Western Core Box site, and collected from bongo nets at the ICE station. FP (10–15 per replicate filter) were rinsed three times in filtered sea water,

photographed under a microscope to obtain size measurements, filtered onto precombusted glass fiber filters (25 mm diameter GF/F, Whatman) and oven dried at  $50^\circ\text{C}$  for analysis of POC. Filters were subsequently fumed with 37% HCl in a vacuum desiccator for 24 h, and dried for 24 h at  $50^\circ\text{C}$ . Filters and filter blanks were placed in precombusted ( $450^\circ\text{C}$ , 24 h) tin capsules as in Hilton et al. (1986), and POC measured in a CE-440 Elemental analyser (Exeter Analytical.285 Inc). These experimentally derived values ( $0.022\text{--}0.058 \text{ mg C mm}^{-3}$ ) compare to literature values for euphausiid FP, which range from  $0.016 \text{ mg C mm}^{-3}$  for FP collected in sediment traps in the upper 100 m in Norway (González 1992), to  $0.0306 \text{ mg C mm}^{-3}$  for FP produced from egestion experiments from *E. superba* collected from the Antarctic marginal ice zone (Suzuki et al. 2001).

#### Statistical analysis

To examine attenuation of POC with depth we fitted regression lines to the data using the statistical package R. The significance of calculated remineralization length scales and Martin's  $b$  values were assessed via calculated  $r^2$  and  $p$  values. Results for exponential and Martin (power law) fits were similar, (e.g., at P2; exponential,  $r^2 = 0.84$ ,  $p < 0.001$  and power,  $r^2 = 0.84$ ,  $p = 0.001$ , and at P3; exponential,  $r^2 = 0.71$ ,  $p = 0.018$  and power,  $r^2 = 0.70$ ,  $p = 0.020$ ), so we use exponential fits as they are less sensitive to the choice of reference depth (Buesseler and Boyd 2009). Intersite differences between sinking velocities of particles, and in particular of FP, were assessed via Student's  $t$ -tests and Mann-Whitney  $U$ -tests, after first testing data for normality and variance homogeneity. Trends between FP size (length, width, volume, or ESD) and carbon-specific respiration rate were assessed via a linear model fit in R, and differences in carbon-specific respiration rates between sites evaluated via a Student's  $t$ -test. Results were considered significant only at the 95% level (i.e., when  $p < 0.05$ ).

## Results

### Hydrography and surface Chlorophyll $a$

Near surface Chl  $a$  from the underway system ranged from  $0.34 \text{ mg m}^{-3}$  to  $6.68 \text{ mg m}^{-3}$  with the highest values occurring near P3. Near surface (5 m) samples from vertical CTD profiles display the same trend with highest concentrations ( $3.31\text{--}5.21 \text{ mg m}^{-3}$ ) at P3 and low concentrations at P2 and ICE ( $0.61\text{--}0.76 \text{ mg m}^{-3}$  and  $0.81\text{--}1.01 \text{ mg m}^{-3}$  respectively). Despite the limitations of cloud cover, satellite data suggest that P3 was sampled during the start of the spring bloom with surface Chl  $a$  concentrations doubling by mid-January. Conversely the ICE station was sampled before the seasonal peak at the end of December, and limited data at P2 suggest that surface Chl  $a$  was in decline when sampled.

Surface temperatures (averaged over the upper 5 m) ranged from  $-0.81^\circ\text{C}$  at ICE,  $0.89^\circ\text{C}$  at P2, and  $2.47^\circ\text{C}$  at P3

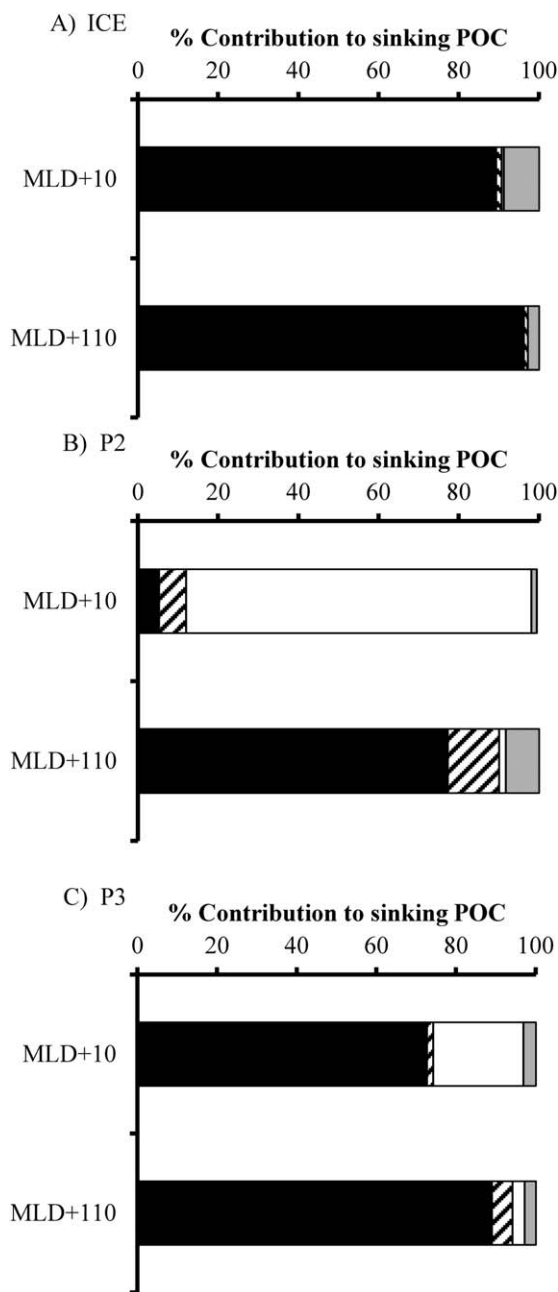


**Fig. 3.** Composition of fast sinking POC at (A) ICE, (B) P2, and (C) P3 stations based on microscope analysis and calculated carbon content. Black = faecal pellets, hashed = phytodetrital aggregates, white = phytoplankton cells, and grey = other. MLD+10 and MLD+110 represent measurements at 10 m and 110 m below the base of the mixed layer depth (MLD), respectively.

(Fig. 1–inset). Temperatures in the Western Core Box ranged from 1.1 to 3.8, averaging 1.9°C.

**Sinking material**

Sinking phytoplankton cells (Fig. 2C) numerically dominated the POC flux at MLD+10 at P2 and P3, whereas FP

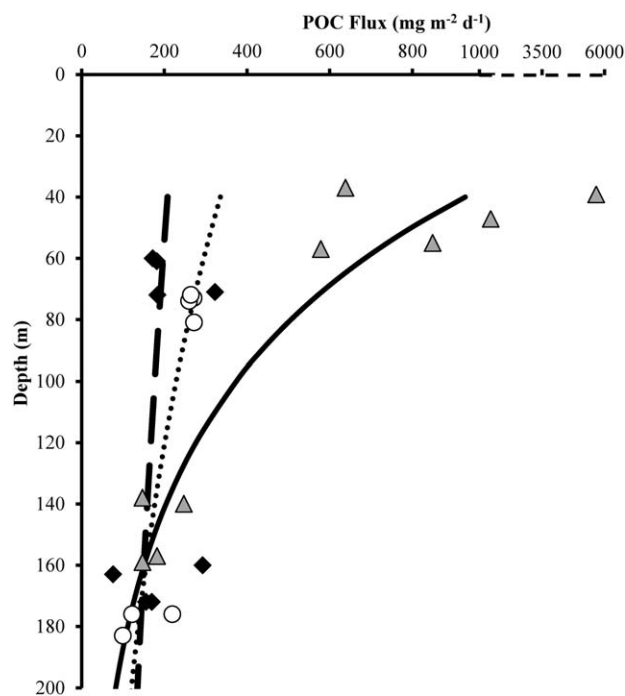


**Fig. 4.** Flux of particulate organic carbon (POC  $\text{mg m}^{-2} \text{d}^{-1}$ ) measured at a number of time points over the diel cycle at ICE (black diamonds), P2 (grey triangles) and P3 (open circles) in the Scotia Sea Antarctica. Exponential curves have been plotted for ICE (thick black dashed), P2 (solid black) and P3 (dotted) to illustrate flux attenuation,  $p < 0.001$ , 0.018, and 0.419 at P2, P3 and ICE, respectively. Note the break in the x axis scale for extreme value at P2 which has been excluded from the exponential fit.

were dominant at ICE. However, in terms of carbon content, FP dominated POC flux (66.7–96.3%) at all depths and stations, with the exception of MLD+10 at P2, where phytoplankton cells accounted for 86.1% of the flux (Fig. 3). Phytodetrital aggregates (Fig. 2B) were a minor component of the POC flux, accounting for <10% at all stations.

**POC flux**

Particle sinking velocities ranged from 2  $\text{m d}^{-1}$  to 570  $\text{m d}^{-1}$  with average velocities of 151  $\text{m d}^{-1}$ , 144  $\text{m d}^{-1}$ , and 88  $\text{m d}^{-1}$  at ICE, P2, and P3 respectively. However, intra site variability was large (2–507  $\text{m d}^{-1}$ , 9–570  $\text{m d}^{-1}$ , and 13–371  $\text{m d}^{-1}$  at ICE, P2, and P3 respectively) reflecting the range of particle types, shapes, and densities. Sinking velocity distributions were non-normal and only P3 and ICE were found to be statistically different (Mann-Whitney  $U$ -test,  $p = 0.006$ ). Sinking velocity measurements were limited to those particles visible by eye ( $\text{ESD} > 0.15 \text{ mm}$ ) and hence averages are an upper estimate. Measured velocities do however agree well with previous measurements in the Southern Ocean ranging from 50  $\text{m d}^{-1}$  to 430  $\text{m d}^{-1}$  (Fischer and Karakas 2009; Cavan et al. 2015).

POC fluxes at the base of the mixed layer (MLD+10) ranged from 172  $\text{mg C m}^{-2} \text{d}^{-1}$  at ICE, to 1454  $\text{mg C m}^{-2}$

$\text{d}^{-1}$  at P2 (Fig. 4). One significantly higher value ( $5668 \text{ mg C m}^{-2} \text{ d}^{-1}$ ) was observed at P2 due to the occurrence of siphonophore remains in the sample, highlighting the high temporal variability and episodic nature of flux events. Exponential curves have been fitted to flux data (Fig. 4), providing a statistically significant fit at P2 ( $p < 0.001$ ) and P3 ( $p = 0.018$ ), but not at ICE ( $p = 0.419$ ) where flux attenuation was low and even negative in one case. The extreme POC flux observed at P2 was excluded from this fit.

Flux attenuation between MLD+10 and MLD+110 was quite variable, both spatially and temporally. Rapid POC flux attenuation was measured at P2, with  $T_{100}$  from 2.6% to 38.8% (average 18%, and  $b$  value 1.60), with slower remineralization at P3 ( $T_{100}$  from 36.7% to 80.9%, average 55%, and  $b$  value 0.78). The highest  $T_{100}$  values and hence highest transfer efficiencies occurred at the ICE station (maximum  $T_{100}$  of 84.9% and  $b$  of 0.19) and, at one time point, the flux actually increased with depth. Calculation of  $T_{100}$  values based on average POC fluxes at MLD+10 and MLD+110 at each station revealed the same trend, with higher attenuation at P2 ( $T_{100} = 20.6\%$ ,  $b = 1.43$ ), and lower attenuation at P3 and ICE ( $T_{100} = 55.1\%$ ,  $b = 0.69$ , and  $T_{100} = 80.7\%$ ,  $b = 0.23$ , respectively). The range in measured sinking velocities was large and without full knowledge of the particle spectrum adds uncertainty to our POC flux calculations. Therefore, a sensitivity analysis has been performed to assess the influence of changing sinking rates on POC flux. Recalculating POC fluxes based on average sinking rates  $\pm$  one standard error, result in POC fluxes changing by just  $\pm 12$ –15% providing confidence in the calculated attenuation rates.

### Fecal pellet flux

Microscope analysis of particles collected in MSC revealed two clear morphological types of FP, cylindrical and round, with cylindrical FP dominating at ICE and P3 stations (80–100%) and round FP being more important at P2 (63–78%). A couple of ellipsoidal FP were also observed at P2 and ICE. FP ranged in colour: dark orange, brown, yellow and white/translucent, but there were no clear trends with depth or station. Average FP size was lower at P2 and P3 (ESD = 0.25 mm and 0.24 mm, respectively), compared to ICE (ESD = 0.31 mm), due to the dominance of cylindrical FP at ICE. Cylindrical FP was significantly larger (ESD = 0.29 mm) than round FP (ESD = 0.21 mm) across all sites (Student's  $t$ -test  $p < 0.05$ ).

Sinking velocities of FP at P3 (average  $88 \text{ m d}^{-1}$ ) were statistically lower than those at P2 and ICE ( $195 \text{ m d}^{-1}$  and  $168 \text{ m d}^{-1}$ , respectively, Mann-Whitney  $U$ -test  $p < 0.005$ ), however data were limited to 10 measurements at P2. FP POC fluxes showed similar patterns of decline as observed for the POC fluxes, with higher attenuation at P2 and P3 ( $T_{100}$  of 59% and 42% respectively) compared to ICE where only a slight decrease in FP POC flux was measured ( $T_{100} = 93\%$ ). Despite a decrease in abundance of FP with depth at each station, the percentage contribution of FP increased, due primarily to the

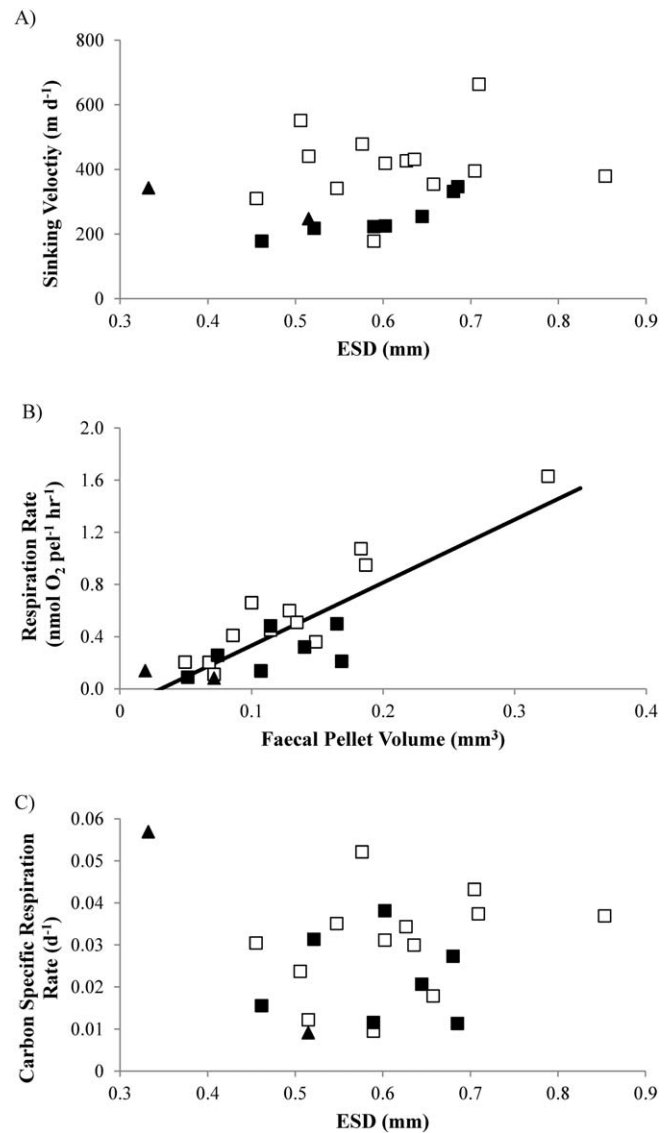


**Fig. 5.** Sinking velocities and respiration rates of FP collected at the West-ern Core Box (open squares), ICE (filled squares), and P2 (filled triangles) stations. (A) FP sinking velocity vs. equivalent spherical diameter (ESD), (B) FP respiration rate vs. FP volume with linear fit ( $Y = 4.8208X - 0.1497$ ,  $R^2 = 0.56$  (Pearson's correlation),  $p < 0.001$ ), (C) Carbon-specific respiration rates vs. FP ESD (no significant relationship,  $p > 0.05$ ).

rapid decrease in the number of sinking phytoplankton cells, suggesting a higher transfer efficiency of FP, an additional deeper source of FP or diel vertical migration.

### Microbial respiration rates

FP used for respiration experiments were predominantly cylindrical, with the exception of one round FP (0.37 mm diameter) collected at P2 from the marine snow catcher. At ICE and P3 cylindrical FP accounted for  $>80\%$  of FP and our data are thus broadly representative of the mean conditions at those stations. Our data may be less applicable to P2

**Table 1.** Size and respiration rates of FP measured in the Scotia Sea, Antarctica.

|         | FP volume<br>( $\times 10^7 \mu\text{m}^3$ ) | FP sinking<br>velocity<br>( $\text{m d}^{-1}$ ) | POC: volume<br>ratio<br>( $\text{mg C mm}^{-3}$ ) | Total O <sub>2</sub><br>consumption<br>( $\text{nmol O}_2$<br>$\text{FP}^{-1} \text{h}^{-1}$ ) | Volumetric O <sub>2</sub><br>consumption<br>( $\text{fmol O}_2$<br>$\mu\text{m}^{-3} \text{d}^{-1}$ ) | Carbon<br>respiration rate<br>( $\text{ng C}$<br>$\text{FP}^{-1} \text{h}^{-1}$ ) | Carbon-specific<br>respiration<br>rate ( $\text{d}^{-1}$ ) |
|---------|--|---|---|--|---|---|--|
| Average | 11.9   | 351   | 0.036   | 0.433  | 0.085   | 5.19  | 0.028  |
| Maximum | 32.5   | 663   | 0.058   | 1.630  | 0.172   | 19.56   | 0.065  |
| Minimum | 1.9  | 177   | 0.022   | 0.082  | 0.028   | 0.98  | 0.010  |

where round FP were dominant and we suggest respiration measurements on other FP morphologies as an important area of further research. Cylindrical FP used in respiration experiments ranged in length from 0.95 mm to 5.37 mm, (average 2.01 mm), and in width from 0.21 mm to 0.42 mm (average 0.28 mm). Sinking velocities of FP used for respiration measurements were between  $177 \text{ m d}^{-1}$  and  $663 \text{ m d}^{-1}$  (average  $351 \text{ m d}^{-1}$ ) (Fig. 5A, Table 1). Sinking velocities of FP collected at the Western Core Box site were higher (average  $413 \text{ m d}^{-1}$ ) than those from ICE and P2 stations (average  $263 \text{ m d}^{-1}$ ) (Student's *t*-test  $p < 0.005$ ).

The carbon content of FP ranged from  $0.022 \text{ mg C mm}^{-3}$  to  $0.058 \text{ mg C mm}^{-3}$  which, based on the range of observed FP colours from light yellow to yellow-brown, may reflect variability in the type and abundance of food available for *E. superba*, as well as the feeding state of the individual producing the FP (Urban-Rich et al. 1998). Lighter, translucent FP may be indicative of feeding on detritus, whereas brown colours may indicate feeding on phytoplankton, and lighter brown colours on a mixture of diatoms, protists, and marine snow (Wilson et al. 2008).

In agreement with the one other published study of this kind (Ploug et al. 2008), measured DBLs of FP were thin, ranging from  $23 \mu\text{m}$  to  $98 \mu\text{m}$ . Oxygen concentrations decreased toward the water-pellet interface and, on the occasions where the FP remained intact when penetrated, oxygen concentrations continued to decrease within the FP, but were still well above anoxic conditions. Oxygen fluxes to the FP ranged from  $0.082 \text{ nmol O}_2 \text{ FP}^{-1} \text{ h}^{-1}$  to  $1.630 \text{ nmol O}_2 \text{ FP}^{-1} \text{ h}^{-1}$  (average  $0.433$ ), increasing with FP ESD ( $R^2 = 0.56$  (Pearson's correlation),  $p < 0.001$ ) (Fig. 5B). This corresponds to volumetric fluxes (oxygen flux per unit volume of FP) of  $0.028$ – $0.172 \text{ fmol O}_2 \mu\text{m}^{-3} \text{ d}^{-1}$  (average  $0.085 \text{ fmol O}_2 \mu\text{m}^{-3} \text{ d}^{-1}$ ), and respiration rates of  $0.98$ – $19.56 \text{ ng C FP}^{-1} \text{ h}^{-1}$  (average  $5.19 \text{ ng C FP}^{-1} \text{ h}^{-1}$ ) (Table 1). Respiration rates increased linearly with FP POC, although this is in part due to the constant FP carbon to volume ratio used for each site (see below) and hence reflects the trends shown in Fig. 5B.

## Discussion

### Role of bloom timing in export flux

Highest POC fluxes at the base of the mixed layer (MLD+10) were recorded at P2 despite low surface Chl *a*,

and were likely associated with the declining phase of the bloom (suggested by satellite data). The observed high fluxes out of the euphotic zone at P2, which were composed mainly of individual and chained phytoplankton cells (86%), may have resulted from increased cell death and bloom decline due to nutrient limitation (e.g., Thornton 2002).

The region downstream of the islands of South Georgia (encompassing the P3 site) is characterised by large spring phytoplankton blooms (Borrione and Schlitzer 2013) supported by increased iron supply from the shelf sediments of South Georgia (Nielsdóttir et al. 2012). These large blooms result in high fluxes of material to the deep ocean (Manno et al. 2015), yet we observed low POC fluxes at the base of the mixed layer (2–10 times smaller than at P2) despite high and increasing surface Chl *a*. Lower contributions of phytoplankton cells to sinking POC flux at P3 (25%) support the idea of an actively growing phytoplankton population, and fewer dead and senescent cells sinking out of the euphotic zone. At this early stage of the bloom, decoupling between primary producers and their consumers likely results in a lag between primary production and export, in agreement with model studies predicting a lag of 20–30 d in the Southern Ocean (Henson et al. 2015).

As expected at this time of year (Ward et al. 2012b), low Chl *a* levels were measured at the ICE station, and this early phase of production may explain the observed low fluxes of POC out of the euphotic zone (average  $215 \text{ mg C m}^{-2} \text{ d}^{-1}$ ).

### Particle composition and mesopelagic flux attenuation

The fitted exponential curves (Fig. 4) demonstrate that POC flux attenuation was variable between sites. Rapid attenuation (average  $T_{100}$  value of 20.6%) at P2 resulted in low POC fluxes at MLD+110, despite high fluxes out of the euphotic zone. Material sinking out of the euphotic zone was comprised mostly of individual and small chained phytoplankton cells which have low sinking velocities (Smayda 1970) and are likely to be more labile and easily degraded than FP (Turner 2002; Laurenceau-Cornec et al. 2015).

POC flux attenuation was less rapid at P3, which may in part be explained by higher FP contributions (71% and 89% at MLD+10 and MLD+110, respectively, Fig. 3), most of

which were cylindrical suggesting the importance of larger copepods and euphausiids (Wilson et al. 2013). Despite lower POC fluxes out of the euphotic zone at ICE, fluxes at MLD+110 were comparable to, and at times higher than, those measured at the more productive P2 and P3 sites. Higher  $T_{100}$  values (maximum of 84.9%) suggest efficient transfer through the upper mesopelagic at ICE which again could be explained by a dominance (89–96%) of FP (mostly cylindrical). The opposite trend, lower FP contributions at MLD+110 and higher attenuation, was observed at P2, supporting the theory that the repackaging of sinking phytoplankton cells and phytodetrital aggregates into fast sinking FP by zooplankton may drive higher transfer efficiencies. Manno et al. (2015) measured higher contributions of FP to POC flux in deep (1500–2000 m) sediment traps in spring at P3 (48%) compared to P2 (20%), supporting this hypothesis.

Higher transfer efficiencies with higher contributions of FP could in part be explained by increased FP sinking velocities in comparison to phytoplankton cells (Turner 2002). Average particle sinking velocities were in fact similar at ICE and P2 despite differences in particle flux composition, and were actually lower at P3 than P2 (not statistically significant). However, sinking velocity data are limited and are skewed toward the large end of the particle spectrum as it was only possible to determine sinking velocities of individual phytoplankton cells with  $ESD > 0.15$  mm (average  $85 \text{ m d}^{-1}$ ). Considering the dominance of phytoplankton cells in sinking material at P2, we expect that average sinking velocities would be lower if the full particle spectrum had been measured. POC flux calculations are therefore also an upper estimate based on the operational limitations of sinking velocity measurements.

#### Role of zooplankton in mesopelagic flux attenuation

Intersite differences in flux attenuation may also reflect differences in zooplankton abundance due to both spatial variability and/or contrasting bloom stage. Spring surveys in the Scotia Sea in 2006 showed lower mesozooplankton biomass at P3 compared to P2 ( $13.41 \text{ g DW m}^{-3}$  and  $57.50 \text{ g DW m}^{-3}$ , respectively), as well as lower biomass at more southerly stations (encompassing the ICE station) (Ward et al. 2012a). This would suggest higher FP contributions to the POC flux at P2 than at P3 or ICE, the opposite trend to that observed here. However, zooplankton community composition, diet, migration patterns, as well as bloom timing and coupling with primary production are all important factors to consider rather than just zooplankton abundance.

Previous studies have shown negative relationships between POC export and the presence of microcopepod species such as *Oithona* spp. (Svensen and Nejstgaard 2003; Suzuki et al. 2003). These microcopepod species have a lifestyle based around coprophagy and coprorhexy which limits the export of FP to depth. The biomass of the microcopepod

community (*Oithona* spp., *Oncaea* sp., *Microcalanus* sp., and *Ctenocalanus* sp.) during a previous springtime cruise was five times greater at P2 than at P3 ( $10.14 \text{ g DW m}^{-3}$  and  $2.00 \text{ g DW m}^{-3}$ , respectively, (Ward et al. 2012a, supporting data)) which is in line with the greater levels of attenuation we observed at P2. In support of this, qualitative visual assessment of FP collected in the MSC suggests that FP were more fragmented in the deeper (MLD+110) MSC samples and that cylindrical pellets in particular showed more signs of fragmentation (broken ends or considerable loss of cylindrical structure) at P2 than P3. The way in which krill FP strings are produced makes it difficult to ascertain whether FP ends were broken on production, and limits our ability to make quantitative assessment of fragmentation. We are also not able to distinguish between biotic and abiotic mechanical breakup. However, our qualitative assessments are consistent with sediment trap data indicating a higher degree of fragmentation of cylindrical, round, and ellipsoidal FP at P2 compared with P3 (Manno et al. 2015). Fragmentation of larger FP may not only aid ingestion (both intentional and unintentional) by smaller zooplankton, but may also increase exposure to microbial degradation (Ploug et al. 2008; Svensen et al. 2012) which may in itself be a feeding strategy (“microbial gardening” (Mayor et al. 2014)), resulting in increased attenuation of POC. Data here therefore support the increasing evidence for high attenuation of POC flux and the key role of the recycling mesozooplankton community across large areas of the Southern Ocean (Cavan et al. 2015; Laurenceau-Cornec et al. 2015; Rembauville et al. 2015). Nevertheless, see Poulsen and Kiørboe (2005), Reigstad et al. (2005) and Iversen and Poulsen (2007) for alternative views on the role of small zooplankton in FP degradation suggesting direct ingestion by some species is unlikely and coprorhexy is more important.

FP collected at the ICE station are believed to be derived from *E. superba*, which are known to be common in this marginal ice zone (Hewitt et al. 2004), as well as some contribution from copepod species. The tendency of *E. superba* to form swarms (Hamner et al. 1989) has the potential to support high POC fluxes to the mesopelagic through a “rain” of rapidly sinking FP, some of which would overload and bypass any detrital feeders. In addition to this, diel vertical migration of zooplankton and excretion at depth (Emerson and Roff 1987) may contribute to the dominance of FP in sinking POC at ICE (Fig. 3).

#### Microbial respiration

This study presents the first direct measurements of respiration rates in euphausiid FP in an attempt to understand the key processes driving flux attenuation in the mesopelagic. A few studies have measured microbial respiration of copepod FP (Hansen et al. 1996; Ploug et al. 2008; Shek and Liu 2010; Köster et al. 2014; Svensen et al. 2014), only one

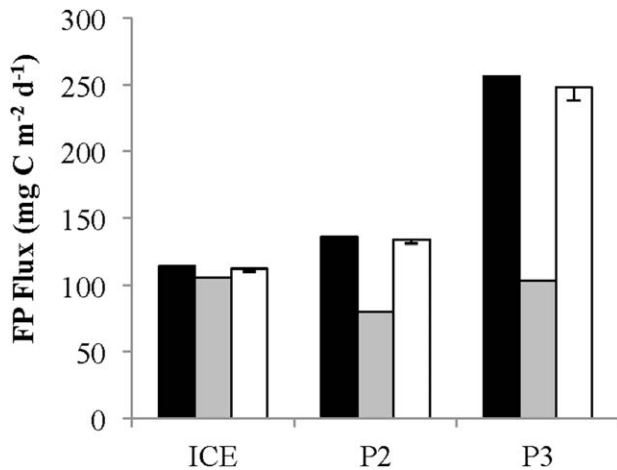


**Fig. 6.** Comparison of FP fluxes measured at MLD+10 (black) and MLD+110 (grey), to those predicted at MLD+110 (white). MLD+10 and MLD+110 represent measurements at 10 m and 110 m below the base of the mixed layer depth (MLD) respectively. Predicted fluxes are based on measured FP fluxes at MLD+10 and average FP respiration rates ( $0.028 \text{ d}^{-1}$ ) derived during this study. Hence, the predicted fluxes only consider microbial degradation via respiration. Error bars show minimum predicted values using minimum literature values for euphausiid FP POC content (González 1992). FP POC contents measured in this study lie at the upper end of literature estimates and hence there is no upper error bar.

of which utilizes the direct methods used here (Ploug et al. 2008).

To calculate the carbon-specific respiration rate, which is essentially a measure of FP remineralization by particle associated microbes, the carbon respiration rate was divided by the FP POC content. For ICE and Western Core Box stations it was possible to use values derived from additional FP collected at the same site (see methods), however at P2, where insufficient FP were available for direct measurement, the FP POC content measured at ICE ( $0.032 \text{ mg C mm}^{-3}$ ) was used. The lack of direct measurement of FP POC at P2 increases the uncertainty in our estimate of carbon-specific respiration rate of FP at P2, but as it was only possible to measure respiration rates on two FP at this site we do not believe that this uncertainty significantly affects conclusions drawn here which utilize average respiration rates across all sites.

Carbon-specific respiration rates were low, ranging from  $0.010 \text{ d}^{-1}$  to  $0.065 \text{ d}^{-1}$  (average  $0.028 \text{ d}^{-1}$ ) (Fig. 5C). There was no significant trend with FP size (length, width, volume, or ESD), and no significant differences were found in carbon-specific respiration rates between sites (Student's *t*-test  $p > 0.05$ ). Sensitivity tests using alternative FP POC conversions ( $0.016 \text{ mg C mm}^{-3}$  based on sediment traps at 50 m and 100 m González 1992; and  $0.0306 \text{ mg C mm}^{-3}$  based on freshly egested FP Suzuki et al. 2001) give average carbon-specific respiration rates of  $0.063 \text{ d}^{-1}$  and  $0.033 \text{ d}^{-1}$ , respectively (Fig. 6).

Low carbon-specific respiration rates suggest that particle associated microbial respiration plays a minimal role in the attenuation of FP POC flux in the upper mesopelagic of the Scotia Sea, agreeing well with undetectable respiration rates of  $0.01 \pm 0.02 \text{ d}^{-1}$ , measured along the western Antarctic Peninsula (McDonnell et al. 2015). Ploug et al. (2008) conducted experiments on small copepod FP (over 500 times smaller volume than analysed here) at  $15^\circ\text{C}$ , and measured much higher rates of carbon-specific respiration ( $0.08\text{--}0.20 \text{ d}^{-1}$ ). FP size may in part explain differences between studies (Svensen et al. 2014), however we observed no relationship between FP ESD and carbon-specific respiration rate over the small size range of FP measured here ( $0.33\text{--}0.85 \text{ mm}$  ESD). A clear trend of increasing respiration rate (in terms of oxygen flux per FP) with increasing FP ESD and FP volume (Fig. 5B) was however observed; larger FP are able to support larger populations of microbes and hence oxygen fluxes to the FP are expected to be higher. However, the range in carbon-specific respiration rates was relatively small, suggesting that microbial respiration increased with increasing carbon content, and hence reactions are not diffusion limited (Ploug 2001), but rather are limited by substrate, temperature, or surface area.

To assess the importance of microbial respiration for the attenuation of FP POC flux in the mesopelagic, the average measured carbon-specific respiration rate ( $0.028 \text{ d}^{-1}$ ) was used to predict the FP flux at MLD+110 that would result if the only loss was via particle associated microbial respiration (Fig. 6). Calculations were based on the relationship between the remineralization length scale ( $L \text{ (m}^{-1}\text{)}$ ) (Iversen et al. 2010), carbon-specific respiration rate ( $C_{\text{spec}} \text{ (d}^{-1}\text{)}$ ) and sinking velocity ( $w \text{ (m d}^{-1}\text{)}$ ).

$$L = \frac{C_{\text{spec}}}{W} = (-\ln(F_z/F_0)/(z-z_0)) \quad (4)$$

Comparisons to observed FP fluxes at MLD+110, revealed that degradation by particle associated microbes caused very little of the observed alteration of the flux over this depth range and that it is a poor predictor of FP flux at P2 and P3 (Fig. 6). This implies that other mechanisms, such as coprorhexy and coprophagy by zooplankton, were more important in reducing FP flux. Conversely, predicted FP flux at MLD+110 was similar to the measured FP flux at the ICE station suggesting that low flux attenuation here was predominantly due to microbial respiration of the FP, and that other processes were less important at the time of sampling (Fig. 6). FP were the dominant component of POC fluxes (Fig. 3) in particular at ICE and P3 stations, and hence processes dominating the attenuation of FP POC are likely to play an important role in the attenuation of total POC. However, if rates of microbial respiration on sinking phytoplankton cells and detrital aggregates are significantly different to those of FP, this could alter the balance

between zooplankton and microbe driven POC attenuation.

Based on the measured low rates of particle associated microbial respiration, we hypothesize that zooplankton can drive rapid attenuation of the POC flux when zooplankton abundances are high (in particular of the recycling mesozooplankton community) and are tightly coupled with primary production. Temporal and spatial variability in zooplankton abundance and community structure may therefore offer one explanation for variability in POC flux attenuation, but temperature has also been proposed as a controlling mechanism. Marsay et al. (2015) suggest that an increase in remineralization rates by a factor of 2–3 with an increase in temperature of 10°C ( $Q_{10}$  coefficient), as reported for other biological rate processes, could explain the differences in POC attenuation they observed in the North Atlantic and North Pacific. Iversen and Ploug (2013) measured a 3.5 fold increase in carbon-specific respiration rates measured in aggregates at 4°C and 15°C. Applying this factor to adjust respiration rates at 4°C measured in this study, gives rates of 0.032–0.228 d<sup>-1</sup> at 15°C, which is very similar to the range of estimates of Ploug et al. (2008). Temperature controls on rates of respiration may therefore account for differences between rates measured here and in other studies, although other characteristics such as the lability of sinking material may also be key (McDonnell et al. 2015). We do not believe that temperature significantly affects rates of zooplankton fragmentation. Although there are short-term responses to changes in temperature, populations of zooplankton acclimate over longer ecological time-scales such that the species-specific respiration rate of populations in colder waters are similar to those in warmer waters (Saborowski et al. 2002). Given that respiration rates are a good proxy for levels of activity, we do not expect rates of fragmentation by these organisms to be a function of temperature across clines where local populations are acclimated to the ambient temperature. Our results therefore support the conclusions of Marsay et al. (2015), but only in cases where microbial respiration is the dominant control on POC flux attenuation, such as when and where production is low and cannot sustain high zooplankton populations, or when primary producers and consumers are decoupled.

There is some uncertainty in the carbon-specific respiration rates derived here due to the lack of direct measurement of the POC content of individual FP used for respiration experiments. However, calculations based on the range of literature values for euphausiid FP POC cannot produce the observed declines in FP POC (error bars of Fig. 6). Carbon-specific respiration rates would need to be between 4 and 32 times larger than those calculated to match the observed decline in FP POC flux between MLD+10 and MLD+110. Given the measured oxygen fluxes to FP, this would require FP POC contents to be 6, 43, or 34 times smaller than measured here to match observed FP degradation at ICE, P2, and

P3, respectively. This is unlikely considering that minimum reported literature values of POC: volume for FP are 0.016 mg C mm<sup>-3</sup> (González 1992), and that average measurements on the fresh FP made here (0.039 mg C mm<sup>-3</sup>) are similar to measurements made on FP collected from sediment traps at 1500–2000 m at P2 and P3 (0.030 mg C mm<sup>-3</sup>) (Manno et al. 2015).

Respiration rates reported in this study were representative of particle-associated microbes only. Free living microbes may also play a large role in the attenuation of POC. The role of free living bacteria vs. particle-associated bacteria within FP is not yet clear (Cnudde et al. 2013; Turner 2015), and in fact a study by Poulsen and Iversen (2008) demonstrated that free living bacteria did not significantly contribute to FP degradation. Instead protozooplankton were the key organisms for the recycling of copepod FP. It is possible that additional colonisation of FP by free living bacteria in the surface ocean (Thiele et al. 2014) may lead to increased densities of particle associated microbes and increased degradation rates of FP as they sink through the water column (Jing et al. 2012). Fragmentation via zooplankton could also increase FP colonisation, increasing degradation rates. In addition, several studies have shown significant loss of FP carbon to the dissolved organic carbon (DOC) pool, driven by ecto-enzymatic hydrolysis by microbes as well as abiotically via diffusion (Urban-Rich 1999; Møller et al. 2003; Thor et al. 2003). Particle associated microbes can enhance the release of DOC from FP, which would result in more rapid microbially driven attenuation of FP POC than suggested by respiration rates measured here. DOC leakage has been observed to occur rapidly after egestion (Urban-Rich 1999) and hence, depending on the depth of FP production, a significant proportion of this POC loss may have already occurred by MLD+10 thus contributing less to attenuation below this depth. We would require a 40–70% loss of FP POC to account for the observed rapid declines in FP POC between MLD+10 and MLD+110 at P2 and P3, which is not likely to be explained by DOC leakage alone (e.g., Møller et al. 2003, Fig. 2). We believe that a combination of mechanical break up via zooplankton, and enzymatic hydrolysis drive the rapid loss of POC, via a transfer to slowly sinking or suspended POC or DOC. Future studies combining direct measurements of particle associated FP respiration with FP incubations in the presence of free living bacteria are needed to better balance the budget of microbial and zooplankton driven degradation processes.

Microbial respiration may represent a slow background process of degradation of the POC flux, which is always occurring but sometimes overshadowed by intense fragmentation and reworking by zooplankton populations. We hypothesize that at times of high productivity such as during the spring bloom, and when zooplankton are exerting tight grazing control, high production is efficiently grazed

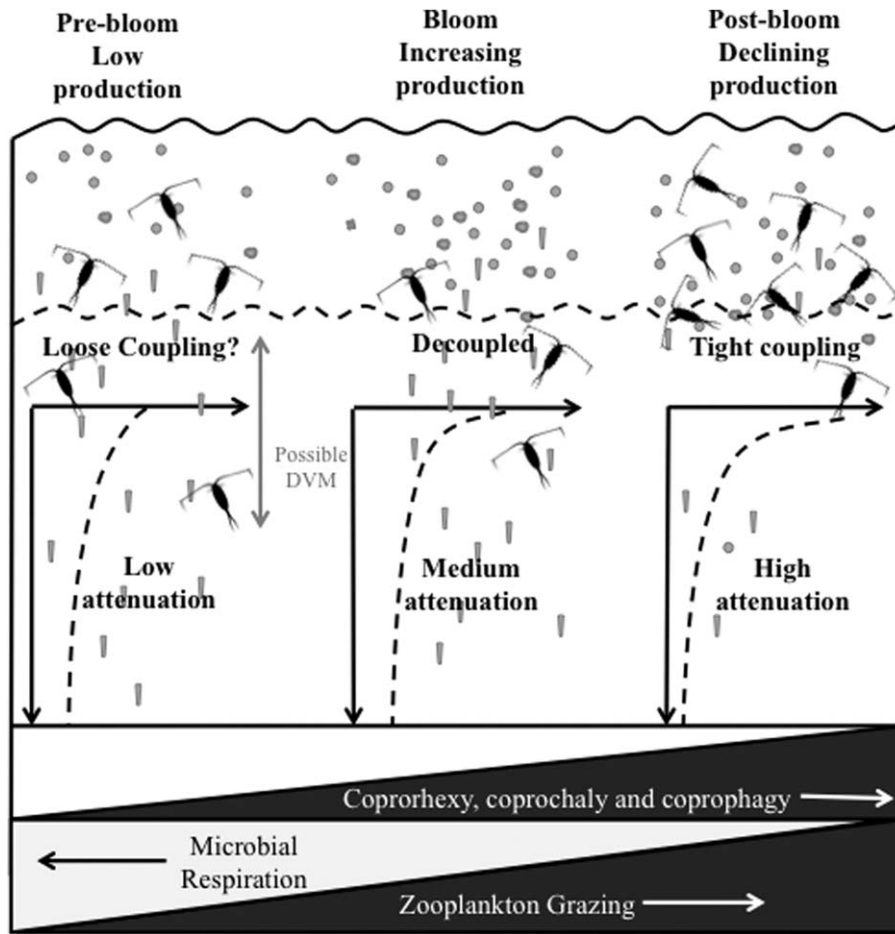


**Fig. 7.** Schematic to illustrate the mechanisms contributing to flux attenuation in the upper mesopelagic in the Scotia Sea, Antarctica, and the influence of bloom phase on these mechanisms.

and recycled in the upper mesopelagic, leading to the high biomass, low export (HBLE) situation noted by Lam and Bishop (2007). Conversely, in prebloom situations, when both algal and zooplankton biomass are low, POC attenuation occurs primarily via microbial respiration (Fig. 7).

**Limitations**

To the best of our knowledge, this is the first study to conduct direct measurements of oxygen gradients, and hence respiration rates, on individual FP in the Southern Ocean. Respiration rates calculated from direct measurements have been used across the study region even though it was not possible to conduct respiration measurements at each station due to the difficulty and time intensive nature of the experiments, as well as operational limitations on FP collection. Therefore, although microbial communities may differ between stations, we present here a best estimate based on the available data.

It was not possible to collect FP from the different sites at the same stage of the bloom, as the blooms in these

regions do not occur concurrently. Variable zooplankton diet, due to different bloom type, may therefore lead to seasonal variability in FP degradation rate, which is not possible to separate from spatial variability in this study. Despite the inevitable uncertainties involved in this, we believe this basin wide compilation provides a good estimate of particle associated microbial respiration in the Scotia Sea. Our data therefore represent a spatial and temporal average and we stress the need for caution before applying these rates to specific regions and at specific stages of the bloom.

**Concluding remarks**

Rates of flux attenuation in the mesopelagic vary widely throughout the global oceans and a number of mechanisms have been proposed to explain these variations. We suggest that high flux attenuation in the upper mesopelagic of the Scotia Sea region is driven by zooplankton, through fragmentation and possible ingestion processes. In these cold regions, microbial respiration is likely to be slow but may

still be important for flux attenuation when zooplankton abundances are low, such as during the prebloom conditions in the marginal ice zone of the South Orkneys. We therefore suggest that temperature may be able to explain global differences in POC flux attenuation, as proposed by Marsay et al. (2015), but only in regions, and at times of the year, where zooplankton abundances are low, and grazing and fragmentation processes are reduced. The stage of the bloom, community structure, and food web interactions are therefore key to determining the rate of POC flux attenuation, and more combined studies measuring POC flux and composition concurrently with ecosystem structure are vital for accurate estimates of the strength of the global biological carbon pump.

### References

- Allredge, A. L. 1998. The carbon, nitrogen and mass content of marine snow as a function of aggregate size. *Deep Sea Res. Part I Oceanogr. Res. Pap.* **45**: 529–541. doi:10.1016/S0967-0637(97)00048-4
- Atkinson, A., K. Schmidt, S. Fielding, S. Kawaguchi, and P. A. Geissler. 2012. Variable food absorption by Antarctic krill: Relationships between diet, egestion rate and the composition and sinking rates of their fecal pellets. *Deep Sea Res. Part II Top. Stud. Oceanogr.* **59–60**: 147–158. doi:10.1016/j.dsr2.2011.06.008
- Berggren, M., J.-F. Lapierre, and P. A. del Giorgio. 2012. Magnitude and regulation of bacterioplankton respiratory quotient across freshwater environmental gradients. *ISME J.* **6**: 984–93. doi:10.1038/ismej.2011.157
- Borrione, I., and R. Schlitzer. 2013. Distribution and recurrence of phytoplankton blooms around South Georgia, Southern Ocean. *Biogeosciences* **10**: 217–231. doi:10.5194/bg-10-217-2013
- Boyd, P. W., and T. W. Trull. 2007. Understanding the export of biogenic particles in oceanic waters: Is there consensus? *Prog. Oceanogr.* **72**: 276–312. doi:10.1016/j.pocean.2006.10.007
- Broecker, W. S., and T. H. Peng. 1974. Gas exchange rates between air and sea. *Tellus* **26**: 21–35. doi:10.1111/j.2153-3490.1974.tb01948.x
- Buesseler, K. O., and P. W. Boyd. 2009. Shedding light on processes that control particle export and flux attenuation in the twilight zone of the open ocean. *Limnol. Oceanogr.* **54**: 1210–1232. doi:10.4319/lo.2009.54.4.1210
- Cavan, E. L., and others. 2015. Attenuation of particulate organic carbon flux in the Scotia Sea, Southern Ocean, controlled by zooplankton fecal pellets. *Geochim. Cosmochim. Acta* **42**: 821–830. doi:10.1002/2014GL062744
- Cnudde, C., C. Sanchez Clavano, T. Moens, A. Willems, and M. De Troch. 2013. Structural and functional patterns of active bacterial communities during aging of harpacticoid copepod fecal pellets. *Aquat. Microb. Ecol.* **71**: 25–42. doi:10.3354/ame01663
- Ebersbach, F., T. W. Trull, D. M. Davies, and S. G. Bray. 2011. Controls on mesopelagic particle fluxes in the Sub-Antarctic and Polar Frontal Zones in the Southern Ocean south of Australia in summer—perspectives from free-drifting sediment traps. *Deep. Res. Part II* **58**: 2260–2276. doi:10.1016/j.dsr2.2011.05.025
- Emerson, C., and J. Roff. 1987. Implications of fecal pellet size and zooplankton behaviour to estimates of pelagic-benthic carbon flux. *Mar. Ecol. Prog. Ser.* **35**: 251–257. doi:10.3354/meps035251
- Fielding, S., J. L. Watkins, M. A. Collins, P. Enderlein, and H. J. Venables. 2012. Acoustic determination of the distribution of fish and krill across the Scotia Sea in spring 2006, summer 2008 and autumn 2009. *Deep. Res. Part II* **59–60**: 173–188. doi:10.1016/j.dsr2.2011.08.002
- Fischer, G., and G. Karakas. 2009. Sinking rates and ballast composition of particles in the Atlantic Ocean: Implications for the organic carbon fluxes to the deep ocean. *Biogeosciences* **6**: 85–102. doi:10.1007/s00531-007-0234-7
- Giering, S. L. C., and others. 2014. Reconciliation of the carbon budget in the ocean's twilight zone. *Nature* **507**: 480–483. doi:10.1038/nature13123
- González, H. E. 1992. The distribution and abundance of krill faecal material and oval pellets in the Scotia and Weddell Seas (Antarctica) and their role in particle flux. *Polar Biol.* **12**: 81–91. doi:10.1007/BF00239968
- Hamner, W., P. Hamner, and B. Obst. 1989. Field observations on the ontogeny of schooling of *Euphausia superba* furcillae and its relationship to ice in Antarctic waters. *Limnol. Oceanogr.* **34**: 451–456. doi:10.4319/lo.1989.34.2.0451
- Hansen, B., F. L. Fotel, N. Jjensen, and S. D. Madsen. 1996. Bacteria associated with a marine planktonic copepod in culture. II. Degradation of fecal pellets produced on a diatom, a nanoflagellate or a dinoflagellate diet. *J. Plankton Res.* **18**: 275–288. doi:10.1093/plankt/18.2.275
- Henson, S. A., R. Sanders, E. Madsen, P. J. Morris, F. Le Moigne, and G. D. Quartly. 2011. A reduced estimate of the strength of the ocean's biological carbon pump. *Geophys. Res. Lett.* **38**: L04606. doi:10.1029/2011GL046735
- Henson, S. A., A. Yool, and R. Sanders. 2015. Variability in efficiency of particulate organic carbon export: A model study. *Global Biogeochem. Cycles* **29**: 33–45. doi:10.1002/2014GB004965
- Hewitt, R. P., and others. 2004. Biomass of Antarctic krill in the Scotia Sea in January/February 2000 and its use in revising an estimate of precautionary yield. *Deep Sea Res. Part II Top. Stud. Oceanogr.* **51**: 1215–1236. doi:10.1016/S0967-0645(04)00076-1
- Hilton, J., J. P. Lishman, S. Mackness, and S. I. Heaney. 1986. An automated method for the analysis of “particulate” carbon and nitrogen in natural waters. *Hydrobiologia* **141**: 269–271. doi:10.1007/BF00014221

- Iversen, M. H., and L. Poulsen. 2007. Coprorhexy, coprophagy, and coprochaly in the copepods *Calanus helgolandicus*, *Pseudocalanus elongatus*, and *Oithona similis*. *Mar. Ecol. Prog. Ser.* **350**: 79–89. doi:10.3354/meps07095
- Iversen, M. H., N. Nowald, H. Ploug, G. A. Jackson, and G. Fischer. 2010. High resolution profiles of vertical particulate organic matter export off Cape Blanc, Mauritania: Degradation processes and ballasting effects. *Deep Sea Res. Part I Oceanogr. Res. Pap.* **57**: 771–784. doi:10.1016/j.dsr.2010.03.007
- Iversen, M. H., and H. Ploug. 2013. Temperature effects on carbon-specific respiration rate and sinking velocity of diatom aggregates—potential implications for deep ocean export processes. *Biogeosciences* **10**: 4073–4085. doi:10.5194/bg-10-4073-2013
- Jing, H., L. Shek, W. Yung, X. Jin, and H. Liu. 2012. Dynamics of bacterial community composition during degradation of copepod fecal pellets. *J. Plankton Res.* **34**: 700–710. doi:10.1093/plankt/fbs043
- Köster, M., G. A. Paffenhöfer, R. Schluter, and A. Meuche. 2014. Time-series observations of prokaryotic colonization of zooplankton fecal pellets. *J. Plankton Res.* **36**: 1461–1475. doi:10.1093/plankt/fbu060
- Kwon, E. Y., F. Primeau, and J. L. Sarmiento. 2009. The impact of remineralization depth on the air–sea carbon balance. *Nat. Geosci.* **2**: 630–635. doi:10.1038/ngeo612
- Lam, P. J., and J. K. B. Bishop. 2007. High biomass, low export regimes in the Southern Ocean. *Deep Sea Res. Part II Top. Stud. Oceanogr.* **54**: 601–638. doi:10.1016/j.dsr2.2007.01.013
- Lampitt, R. S., T. Noji, and B. Von Bodungen. 1990. What happens to zooplankton faecal pellets? Implications for material flux. *Mar. Biol.* **104**: 15–23. doi:10.1007/BF01313152
- Laurenceau-Cornec, E. C., and others. 2015. The relative importance of phytoplankton aggregates and zooplankton fecal pellets to carbon export: Insights from free-drifting sediment trap deployments in naturally iron-fertilised waters near the Kerguelen Plateau. *Biogeosciences* **12**: 1007–1027. doi:10.5194/bg-12-1007-2015
- Manno, C., G. Stowasser, P. Enderlein, S. Fielding, and G. A. Tarling. 2015. The contribution of zooplankton faecal pellets to deep-carbon transport in the Scotia Sea (Southern Ocean). *Biogeosciences* **12**: 1955–1965. doi:10.5194/bg-12-1955-2015
- Marsay, C. M., R. J. Sanders, S. A. Henson, K. Pabortsava, E. P. Achterberg, and R. S. Lampitt. 2015. Attenuation of sinking particulate organic carbon flux through the mesopelagic ocean. *Proc. Natl. Acad. Sci. U. S. A.* **112**: 1089–1094. doi:10.1073/pnas.1415311112
- Martin, J. H., G. A. Knauer, D. M. Karl, and W. W. Broenkow. 1987. VERTEX: Carbon cycling in the north-east Pacific. *Deep Sea Res. Part I Oceanogr. Res. Pap.* **34**: 267–285. doi:10.1016/0198-0149(87)90086-0
- Mayor, D. J., R. Sanders, S. L. C. Giering, and T. R. Anderson. 2014. Microbial gardening in the ocean's twilight zone: Detritivorous metazoans benefit from fragmenting, rather than ingesting, sinking detritus. *Bioessays* **36**: 1132–1137. doi:10.1002/bies.201400100
- McDonnell, A. M. P., P. W. Boyd, and K. O. Buesseler. 2015. Effects of sinking velocities and microbial respiration rates on the attenuation of particulate carbon fluxes through the mesopelagic zone. *Global Biogeochem. Cycles* **29**: 175–193. doi:10.1002/2014GB004935
- Menden-Deuer, S., and E. J. Lessard. 2000. Carbon to volume relationships for dinoflagellates, diatoms, and other protist plankton. *Limnol. Oceanogr.* **45**: 569–579. doi:10.4319/lo.2000.45.3.0569
- Møller, E., P. Thor, and T. Nielsen. 2003. Production of DOC by *Calanus finmarchicus*, *C. glacialis* and *C. hyperboreus* through sloppy feeding and leakage from fecal pellets. *Mar. Ecol. Prog. Ser.* **262**: 185–191. doi:10.3354/meps262185
- Murphy, E. J., and others. 2007. Spatial and temporal operation of the Scotia Sea ecosystem: A review of large-scale links in a krill centred food web. *Philos. Trans. R. Soc. B Biol. Sci.* **362**: 113–148. doi:10.1098/rstb.2006.1957
- Nielsdóttir, M. C., and others. 2012. Seasonal and spatial dynamics of iron availability in the Scotia Sea. *Mar. Chem.* **130–131**: 62–72. doi:10.1016/j.marchem.2011.12.004
- Ploug, H. 2001. Small-scale oxygen fluxes and remineralization in sinking aggregates. *Limnol. Oceanogr.* **46**: 1624–1631. doi:10.4319/lo.2001.46.7.1624
- Ploug, H., M. Köhl, B. Buchholz-Cleven, and B. B. Jørgensen. 1997. Anoxic aggregates—an ephemeral phenomenon in the pelagic environment? *Aquat. Microb. Ecol.* **13**: 285–294. doi:10.3354/ame013285
- Ploug, H., and B. B. Jørgensen. 1999. A net-jet flow system for mass transfer and microsensor studies of sinking aggregates. *Mar. Ecol. Prog. Ser.* **176**: 279–290. doi:10.3354/meps176279
- Ploug, H., and H.-P. Grossart. 2000. Bacterial growth and grazing on diatom aggregates: Respiratory carbon turnover as a function of aggregate size and sinking velocity. *Limnol. Oceanogr.* **45**: 1467–1475. doi:10.4319/lo.2000.45.7.1467
- Ploug, H., M. H. Iversen, M. Koski, and E. T. Buitenhuis. 2008. Production, oxygen respiration rates, and sinking velocity of copepod fecal pellets: Direct measurements of ballasting by opal and calcite. *Limnol. Oceanogr.* **53**: 469–476. doi:10.4319/lo.2008.53.2.0469
- Ploug, H., A. Terbruggen, A. Kaufmann, D. Wolf-gladrow, and U. Passow. 2010. A novel method to measure particle sinking velocity in vitro, and its comparison to three other in vitro methods. *Limnol. Oceanogr.: Methods* **8**: 386–393. doi:10.4319/lom.2010.8.386
- Poulsen, L., and T. Kiørboe. 2005. Coprophagy and coprorhexy in the copepods *Acartia tonsa* and *Temora*

- longicornis: Clearance rates and feeding behaviour. *Mar. Ecol. Prog. Ser.* **299**: 217–227. doi:10.3354/meps299217
- Poulsen, L., and M. H. Iversen. 2008. Degradation of copepod fecal pellets: Key role of protozooplankton. *Mar. Ecol. Prog. Ser.* **367**: 1–13. doi:10.3354/meps07611
- Prairie, J., and others. 2013. Delayed settling of marine snow at sharp density transitions driven by fluid entrainment and diffusion-limited retention. *Mar. Ecol. Prog. Ser.* **487**: 185–200. doi:10.3354/meps10387
- Reigstad, M., C. W. Riser, and C. Svensen. 2005. Fate of copepod faecal pellets and the role of *Oithona* spp. *Mar. Ecol. Prog. Ser.* **304**: 265–270. doi:10.3354/meps304265
- Rembauville, M., I. Salter, N. Leblond, A. Gueneugues, and S. Blain. 2015. Export fluxes in a naturally iron-fertilized area of the Southern Ocean—part 1: Seasonal dynamics of particulate organic carbon export from a moored sediment trap. *Biogeosciences* **12**: 3153–3170. doi:10.5194/bg-12-3153-2015
- Revsbech, N. P. 1989. An oxygen microsensor with a guard cathode. *Limnol. Oceanogr.* **34**: 474–478. doi:10.4319/lo.1989.34.2.0474
- Riley, J. S., R. Sanders, C. Marsay, F. Le Moigne, E. P. Achterberg, and A. J. Poulton. 2012. The relative contribution of fast and slow sinking particles to ocean carbon export. *Global Biogeochem. Cycles* **26**: GB1026. doi:10.1029/2011GB004085
- Roe, H. S. J., and D. M. Shale. 1979. A new multiple rectangular midwater trawl (RMT 1 + 8M) and some modifications to the institute of oceanographic sciences' RMT 1 + 8. *Mar. Biol.* **50**: 283–288. doi:10.1007/BF00394210
- Saborowski, R., S. Bröhl, G. A. Tarling, and F. Buchholz. 2002. Metabolic properties of Northern krill, *Meganyctiphanes norvegica*, from different climatic zones. I. Respiration and excretion. *Mar. Biol.* **140**: 547–556. doi:10.1007/s00227-001-0730-4
- Shek, L., and H. Liu. 2010. Oxygen consumption rates of fecal pellets produced by three coastal copepod species fed with a diatom *Thalassiosira pseudonana*. *Mar. Pollut. Bull.* **60**: 1005–1009. doi:10.1016/j.marpolbul.2010.02.001
- Smayda, T. J. 1970. The suspension and sinking of phytoplankton in the sea. *Oceanogr. Mar. Biol. Annu. Rev.* **8**: 353–414. ISBN: 0080345085.
- Steinberg, D. K., B. A. S. Van Mooy, K. O. Buesseler, P. W. Boyd, and D. M. Karl. 2008. Bacterial vs. zooplankton control of sinking particle flux in the ocean's twilight zone. *Limnol. Oceanogr.* **53**: 1327–1338. doi:10.4319/lo.2008.53.4.1327
- Suzuki, H., H. Sasaki, and M. Fukuchi. 2001. Short-term variability in the flux of rapidly sinking particles in the Antarctic marginal ice zone. *Polar Biol.* **24**: 697–705. doi:10.1007/s003000100271
- Suzuki, H., H. Sasaki, and M. Fukuchi. 2003. Loss processes of sinking fecal pellets of zooplankton in the mesopelagic layers of the Antarctic marginal ice zone. *J. Oceanogr.* **59**: 809–818. doi:10.1023/B:JOCE.0000009572.08048.0d
- Svensen, C., and J. C. Nejstgaard. 2003. Is sedimentation of copepod faecal pellets determined by cyclopoids? Evidence from enclosed ecosystems. *J. Plankton Res.* **25**: 917–926. doi:10.1093/plankt/25.8.917
- Svensen, C., C. Wexels Riser, M. Reigstad, and L. Seuthe. 2012. Degradation of copepod faecal pellets in the upper layer: Role of microbial community and *Calanus finmarchicus*. *Mar. Ecol. Prog. Ser.* **462**: 39–49. doi:10.3354/meps09808
- Svensen, C., N. Morata, and M. Reigstad. 2014. Increased degradation of copepod faecal pellets by co-acting dinoflagellates and *Centropages hamatus*. *Mar. Ecol. Prog. Ser.* **516**: 61–70. doi:10.3354/meps10976
- Thiele, S., B. M. Fuchs, R. Amann, and M. H. Iversen. 2014. Colonization in the photic zone and subsequent changes during sinking determines bacterial community composition in marine snow. *Appl. Environ. Microbiol.* **81**: 1–34. doi:10.1128/AEM.02570-14
- Thor, P., H. Dam, and D. Rogers. 2003. Fate of organic carbon released from decomposing copepod fecal pellets in relation to bacterial production and ectoenzymatic activity. *Aquat. Microb. Ecol.* **33**: 279–288. doi:10.3354/ame033279
- Thornton, D. C. O. 2002. Diatom aggregation in the sea: Mechanisms and ecological implications. *Eur. J. Phycol.* **37**: 149–161. doi:10.1017/S0967026202003657
- Turner, J. T. 2002. Zooplankton fecal pellets, marine snow and sinking phytoplankton blooms. *Aquat. Microb. Ecol.* **27**: 57–102. doi:10.3354/ame027057
- Turner, J. T. 2015. Zooplankton fecal pellets, marine snow, phytodetritus and the ocean's biological pump. *Prog. Oceanogr.* **130**: 205–248. doi:10.1016/j.pocean.2014.08.005
- Urban-Rich, J. 1999. Release of dissolved organic carbon from copepod fecal pellets in the Greenland Sea. *J. Exp. Mar. Bio. Ecol.* **232**: 107–124. doi:10.1016/S0022-0981(98)00104-X
- Urban-Rich, J., D. A. Hansell, and M. R. Roman. 1998. Analysis of copepod fecal pellet carbon using a high temperature combustion method. *Mar. Ecol. Prog. Ser.* **171**: 199–208. doi:10.3354/meps171199
- Volk, T., and M. I. Hoffert. 1985. Ocean carbon pumps: Analysis of relative strengths and efficiencies in ocean driven atmospheric CO<sub>2</sub> changes, p. 99–110. *In* E. T. Sundquist and W. S. Broecker [eds.], *The carbon cycle and atmospheric CO<sub>2</sub>: Natural variations Archean to Present*. American Geophysical Union.
- Ward, P., A. Atkinson, and G. Tarling. 2012a. Mesozooplankton community structure and variability in the Scotia Sea: A seasonal comparison. *Deep Sea Res. Part II Top. Stud. Oceanogr.* **59–60**: 78–92. doi:10.1016/j.dsr2.2011.07.004
- Ward, P., and others. 2012b. Food web structure and bioregions in the Scotia Sea: A seasonal synthesis. *Deep Sea Res. Part II Top. Stud. Oceanogr.* **59–60**: 253–266. doi:10.1016/j.dsr2.2011.08.005

- Wilson, S. E., D. K. Steinberg, and K. O. Buesseler. 2008. Changes in fecal pellet characteristics with depth as indicators of zooplankton repackaging of particles in the mesopelagic zone of the subtropical and subarctic North Pacific Ocean. *Deep Sea Res. Part II Top. Stud. Oceanogr.* **55**: 1636–1647. doi:[10.1016/j.dsr2.2008.04.019](https://doi.org/10.1016/j.dsr2.2008.04.019)
- Wilson, S. E., H. A. Ruhl, and K. L. Smith. 2013. Zooplankton fecal pellet flux in the abyssal northeast Pacific: A 15 year time-series study. *Limnol. Oceanogr.* **58**: 881–892. doi:[10.4319/lo.2013.58.3.0881](https://doi.org/10.4319/lo.2013.58.3.0881)

### Acknowledgments

We thank the officers and crew of the RRS *James Clark Ross* for their help and support at all hours during cruise JR304. In addition, we would like to thank the scientific party aboard the cruise, in particular Manon

Duret for her help with deployments, Sophie Fielding for her assistance with CTD processing and Jenny Thomas for data management. Thank you all for your words of encouragement, technical expertise and friendship during long shifts on station. We would also like to thank the three anonymous reviewers for their insights and suggestions. This work supported through Natural Environment Research Council National Capability funding to Stephanie Henson and Richard Sanders, National Oceanography Centre and to Geraint Tarling and Clara Manno, British Antarctic Survey. Fieldwork was supported by a Collaborative Gearing Scheme grant to Stephanie Henson.

*Submitted 31 July 2015*

*Revised 12 November 2015; 8 January 2016*

*Accepted 11 January 2016*

*Associate editor: Thomas Kiørboe*